

## Electronic Supplementary Information

# Hemi-core@Frame AuCu@IrNi Nanocrystals as Active and Durable Bifunctional Catalysts for the Water Splitting Reaction in Acidic Media

Jongsik Park,<sup>a†</sup> Songa Choi,<sup>a†</sup> Aram Oh,<sup>b</sup> Haneul Jin,<sup>a</sup> Jinwhan Joo,<sup>a</sup> Hionsuck Baik,<sup>b</sup> and  
Kwangyeol Lee<sup>\*a</sup>

<sup>a</sup>Department of Chemistry, Korea University, Seoul 02841, Korea

<sup>b</sup>Korea Basic Science Institute (KBSI), Seoul 02841, Korea

<sup>†</sup>These authors contributed equally to this work.

## **Experimental Section**

### **Chemical and Materials**

HAuCl<sub>4</sub>•xH<sub>2</sub>O and Ir(acac)<sub>3</sub> (98%) was purchased from STREM Chemicals. Sodium acetate, Ni(acac)<sub>2</sub> (95%), Cu(acac)<sub>2</sub> (99.9%), 1,2-HDD (technical grade, 90%), oleylamine (technical grade, 70%), and oleylamine (98%) were purchased from Sigma-Aldrich. CTAC was purchased from Alfa-Aesar. All reagents were used as received without further purification. Commercial Ir/C (20 wt% on Vulcan XC-72) was purchased from Premetek and commercial Pt/C (20 wt% on carbon black, HiSPEC 3000) was purchased from Alfa Aesar.

### **Material Characterization**

TEM and HRTEM studies were carried out in a TECNAI G2 F30ST microscope and Tecnai G2 20 S-twin microscope. Aberration-corrected imaging and high spatial resolution EDS were performed at FEI Nanoport in Eindhoven using a Titan Probe Cs TEM 300kV with Chemi-STEM technology. EDS elemental mapping data were collected using a higher efficiency detection system (Super-X detector with XFEG); it integrates 4 FEI-designed Silicon Drift Detectors (SDDs) very close to the sample area. Compared to conventional EDX detector with Schottky FEG systems, ChemiSTEM produces up to 5 times the X-ray generation with the X-FEG, and up to 10 times the X-ray collection with the Super-X detector. All scanning transmission electron microscopy (STEM) images and compositional maps were acquired with the use of HAADF-STEM. Powder X-ray diffraction (PXRD) patterns were collected to understand the crystal structures of Ir-based nanocrystals with a Rigaku Ultima III diffractometer system using a graphite-monochromatized Cu-K $\alpha$  radiation at 40 kV and 40 mA.

### **Preparation of Au Seed**

After a slurry of HAuCl<sub>4</sub> (0.08 mmol) was dissolved in 8 mL of oleylamine (technical grade, 70%) to make a gold stock solution, sodium acetate (4.0 mmol) and oleylamine (technical grade, 70%) (82.7 mmol) was prepared in a 500 mL Schlenk tube with magnetic stirrer, and then the 0.08 mmol of gold stock solution was injected to the prepared 500 mL Schlenk tube. After the solution was placed under vacuum at room temperature for 5 min, the reaction mixture maintained at RT under Ar atmosphere, equipped with a bubbler. When Ar gas was fully injected to the 500 mL

Schlenk tube, Ar gas injection was stopped, and the solution was kept at 120 °C for 2 h under 1 atm of Ar gas. The product was cooled to room temperature, and then added with 20 mL of toluene and 108 mL of methanol was centrifuged at 4000 rpm for 5 min. The resulting Au seeds were dispersed in 8 mL of oleylamine (98%).

### **Preparation of AuCu@IrNi Core@Shell nanoparticles (ACIN-CS)**

A slurry of Ir(acac)<sub>3</sub> (0.02 mmol), Ni(acac)<sub>2</sub> (0.02 mmol), Cu(acac)<sub>2</sub> (0.02 mmol), CTAC (0.08 mmol), 1,2-HDD (0.04 mmol), oleylamine (98%) (12 mmol) and prepared Au seed (0.01 mmol) was prepared in a 100 mL Schlenk tube with magnetic stirrer. After the solution was placed under air at 60 °C for 5 min, the Schlenk tube was directly placed in a hot oil bath, which was preheated to 260 °C. After being heated at the same temperature 40 min, the reaction mixture was cooled to room temperature with magnetic stirring. The reaction mixture, after being cooled to room temperature and adding 15 mL of toluene and 25 mL of ethanol, was centrifuged at 4000 rpm for 5 min. The resulting precipitates were dispersed in 2 mL of toluene and 2 mL of ethanol and then mixed with 2 mL of 3 M HCl solution. The mixture was placed at 60 °C for 1 h. Finally, the precipitated ACIN-CS, after being cooled to room temperature and adding 25 mL of ethanol, was centrifuged at 3500 rpm for 5 min. The resulting precipitates were dispersed in 2 mL of oleylamine. After adding 15 mL of toluene and 25 mL of ethanol, the mixture was centrifuged at 4000 rpm for 5 min and then dried under vacuum.

### **Preparation of AuCu Seed**

After a slurry of HAuCl<sub>4</sub> (0.08 mmol) was dissolved in 8 mL of oleylamine (technical grade, 70%) to make a gold stock solution, sodium acetate (4.0 mmol) and oleylamine (technical grade, 70%) (82.7 mmol) was prepared in a 500 mL Schlenk tube with magnetic stirrer, and then the 0.08 mmol of gold stock solution was injected to the prepared 500 mL Schlenk tube. After the solution was placed under vacuum at room temperature for 5 min, the reaction mixture maintained at RT under Ar atmosphere, equipped with a bubbler. When Ar gas was fully injected to the 500 mL Schlenk tube, Ar gas injection was stopped, and the solution was kept at 120 °C for 2 h under 1 atm of Ar gas. After 2 h, Cu(acac)<sub>2</sub> (0.08 mmol) with oleylamine (technical grade, 70%) (24.32 mmol, 8 mL) was injected to the Schlenk tube in reaction raising the temperature up to 280 °C for

1h. The product was cooled to room temperature, and then added with 20 mL of toluene and 108 mL of methanol, was centrifuged at 4000 rpm for 5 min. The resulting AuCu seeds were dispersed in 8 mL of oleylamine (98%).

#### **Preparation of AuCu@IrNi hemi-core@frame nanoparticles (ACIN-HF)**

A slurry of Ir(acac)<sub>3</sub> (0.02 mmol), Ni(acac)<sub>2</sub> (0.04 mmol), CTAC (0.08 mmol), 1,2-HDD (0.04 mmol), oleylamine (98%) (12 mmol) and prepared AuCu seed (0.01 mmol) was prepared in a 100 mL Schlenk tube with magnetic stirrer. After the solution was placed under air at 60 °C for 5 min, the Schlenk tube was directly placed in a hot oil bath, which was preheated to 260 °C. After being heated at the same temperature 40 min, the reaction mixture was cooled to room temperature with magnetic stirring. The reaction mixture, after being cooled to room temperature and adding 15 mL of toluene and 25 mL of ethanol, was centrifuged at 4000 rpm for 5 min. The resulting precipitates (PACIN-HF) were dispersed in 2 mL of toluene and 2 mL of ethanol and then mixed with 2 mL of 3 M HCl solution. The mixture was placed at 60 °C for 1 h. Finally, the precipitated ACIN-HF, after being cooled to room temperature and adding 25 mL of ethanol, was centrifuged at 3500 rpm for 5 min. The resulting precipitates were dispersed in 2 mL of oleylamine. After adding 15 mL of toluene and 25 mL of ethanol, the mixture was centrifuged at 4000 rpm for 5 min and then dried under vacuum.

#### **Preparation of Cu@IrNi single frame nanoparticles (CIN-SF)**

The synthetic method of Cu@IrNi single nanoframe could be found through our previous result.<sup>12</sup> A slurry of Ir(acac)<sub>3</sub> (0.02 mmol), Ni(acac)<sub>2</sub> (0.04 mmol), Cu(acac)<sub>2</sub> (0.02 mmol), CTAC (0.08 mmol), 1,2-HDD (0.04 mmol) and oleylamine (98%) (12 mmol) was prepared in a 100 mL Schlenk tube with magnetic stirrer. After the solution was placed under air at 60 °C for 5 min, the Schlenk tube was directly placed in a hot oil bath, which was preheated to 260 °C. After being heated at the same temperature 40 min, the reaction mixture was cooled to room temperature with magnetic stirring. The reaction mixture, after being cooled to room temperature and adding 15 mL of toluene and 25 mL of ethanol, was centrifuged at 4000 rpm for 5 min. The resulting precipitates were dispersed in 2 mL of toluene and 2 mL of ethanol and then mixed with 2 mL of 3 M HCl solution. The mixture was placed at 60 °C for 1 h. Finally, the precipitated ACIN-HF, after being

cooled to room temperature and adding 25 mL of ethanol, was centrifuged at 3500 rpm for 5 min. The resulting precipitates were dispersed in 2 mL of oleylamine. After adding 15 mL of toluene and 25 mL of ethanol, the mixture was centrifuged at 4000 rpm for 5 min and then dried under vacuum.

### **Preparation of working electrode**

The 10  $\mu\text{g}_{\text{Ir}}$  samples of Vulcan carbon supported catalysts was mixed with 20  $\mu\text{L}$  of Nafion (5 wt%, Sigma-Aldrich), 600  $\mu\text{L}$  of ethanol (anhydrous, Sigma-Aldrich), and 380  $\mu\text{L}$  of D.I. water under sonication at least 30 min in an ice bath. A rotating ring-disk electrode (RRDE) was polished with a 1  $\mu\text{m}$  and 0.05  $\mu\text{m}$  alumina suspension on polishing pad (Buehler); 4  $\mu\text{L}$  of as-prepared ink was dropped on the RRDE (diameter: 4 mm, area: 0.1257  $\text{cm}^2$ ) and spun at 800 rpm for 8 min. Thereafter, the electrode was placed in an oven at 60  $^{\circ}\text{C}$  at 2 min for drying.

### **Electrochemical measurements**

The HER and OER activity test were conducted on an electrochemical workstation (CHI 750E, CH Instruments) in a standard three electrode cell in 0.1 M  $\text{HClO}_4$  (70%, Suprapur grade, Merck) with an electrode rotator at room temperature. A glassy carbon electrode, an Ag/AgCl with saturated KCl, and a graphite rod were used as the working electrode, reference and counter electrode, respectively. All data are presented after conversion to the reversible hydrogen electrode (RHE) scale by measuring open circuit potential of Ag/AgCl with RHE ( $\text{H}^+ | \text{H}_2$  equilibrium on Pt electrode). To measure the resistance, electrochemical impedance spectroscopy (EIS) was performed from 10 kHz to 1 Hz with a potential amplitude of 10 mV. Nyquist plots were determined by the resistance and used for  $iR$ -drop correction.

The overall water splitting test was performed in a two-electrode system in 0.5 M  $\text{H}_2\text{SO}_4$  (96%, Suprapur grade, Merck) at room temperature. All the catalyst inks modified on CFP were used as both cathode and anode in overall water splitting.

### **Measurement of hydrogen evolution reaction (HER) activity**

Before the electrochemical measurement, the electrolyte was purged with highly pure nitrogen gas (99.999%) for 15 min to remove any impurity gas. Electrochemical cleaning was performed

by cyclic voltammetry (CV) in the potential range of 0.05 -1.1 V (vs. RHE) at a scan rate of 500 mV s<sup>-1</sup> for 50 cycles to eliminate residual ligands from the catalyst surface. Before evaluating catalytic activity, 10 CV cycles in HER potential range were performed until the curves became steady. Thereafter, HER activity was evaluated by measuring linear sweep voltammetry (LSV) in the potential range of -0.2 – 0.05 V at a scan rate of 5 mV s<sup>-1</sup>. HER activity was measured under 2500 rpm of electrode rotation because of a rapid hydrogen gas evolution. Electrochemical impedance spectroscopy (EIS) was performed in the frequency range of 10 kHz to 1 Hz at 0 V with an amplitude of 10 mV. The x-intercept of the Nyquist plot in the high frequency region was used for iR-compensation.

### **Measurement of oxygen evolution reaction (OER) activity**

Before the electrochemical measurement, the electrolyte was purged with highly pure nitrogen gas (99.999%) for 15 min to remove any impurity gas. Electrochemical cleaning was performed by cyclic voltammetry (CV) in the potential range of 0.05 -1.1 V (vs. RHE) at a scan rate of 200 mV s<sup>-1</sup> for 20 cycles to eliminate residual ligands from the catalyst surface. Before evaluating catalytic activity, 10 CV cycles in HER potential range were performed until the curves became steady. Thereafter, HER activity was evaluated by measuring linear sweep voltammetry (LSV) in the potential range of 1.1 – 1.7 V at a scan rate of 5 mV s<sup>-1</sup>. OER activity was measured under 1600 rpm of electrode rotation. Electrochemical impedance spectroscopy (EIS) was performed in the frequency range of 10 kHz to 1 Hz at 0 V with an amplitude of 10 mV. The x-intercept of the Nyquist plot in the high frequency region was used for iR-compensation.

### **Measurement of full water splitting activity and stability**

The 0.5 M H<sub>2</sub>SO<sub>4</sub> electrolyte was purged with highly pure nitrogen gas (99.999%) for 15 min to remove any impurity gas. Before measuring overall water splitting activity, electrochemical cleaning was performed by cyclic voltammetry (CV) in the potential range of 0.0 -1.0 V at a scan rate of 500 mV s<sup>-1</sup> for 20 cycles to remove ligands on the electrode surface. Then, LSV was obtained in the potential range of 1.0 - 2.2 V with a scan rate of 50 mV s<sup>-1</sup>. The chronopotentiometry for stability test was measured under a constant current density of 10 mA cm<sup>-2</sup>.

For CO-stripping, CO molecules were adsorbed on the catalyst surface under a constant potential of 0.10 V (vs RHE) for 3 min with 30% CO (Ar-balanced) bubbling, and dissolved CO in the electrolyte was flushed by N<sub>2</sub> bubbling for the next 27 min. Three cycles of CV at a scan rate of 100 mV s<sup>-1</sup> were applied from 0.05 to 1.1 V (vs RHE). The current peak arising in the potential range from 0.7 V to 1.1 V originates from the oxidative desorption of the monolayer CO on the catalyst surface. The peak area corresponds to the CO-stripping charge and the normalization of the value using the known specific charge 420 μC per 1 cm<sup>2</sup> of Ir surface gives the ECSA.

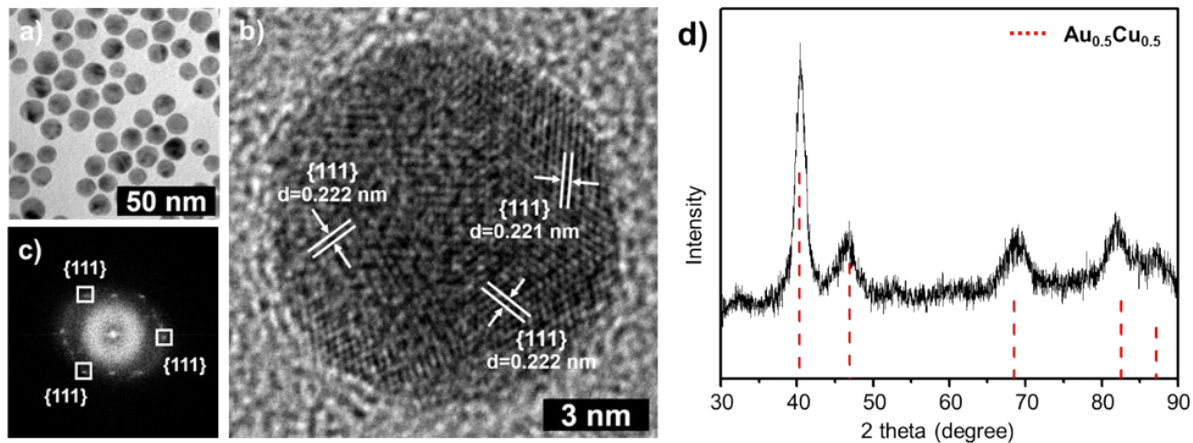


**Fig. S1** Characterization of AuCu seeds. a) TEM, b) HRTEM, and c) corresponding FFT pattern of AuCu seeds. d) The PXRD analysis of AuCu seeds. The red dashed line indicates the  $\text{Au}_{0.5}\text{Cu}_{0.5}$  reference (PDF#01-074-5367).

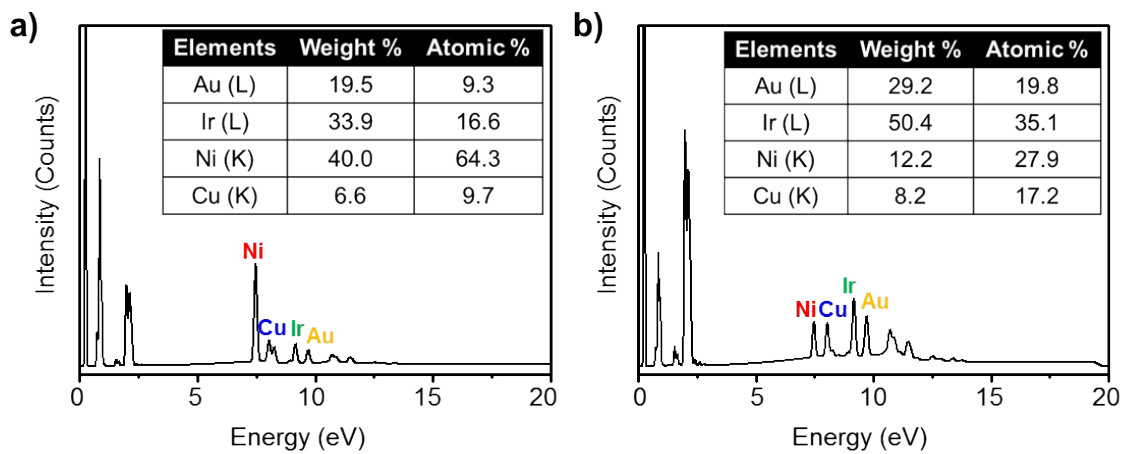


**Fig. S2** EDS spectrums of a) PACIN-HF and b) ACIN-HF. Samples for EDS measurement were prepared on a Mo TEM grid.

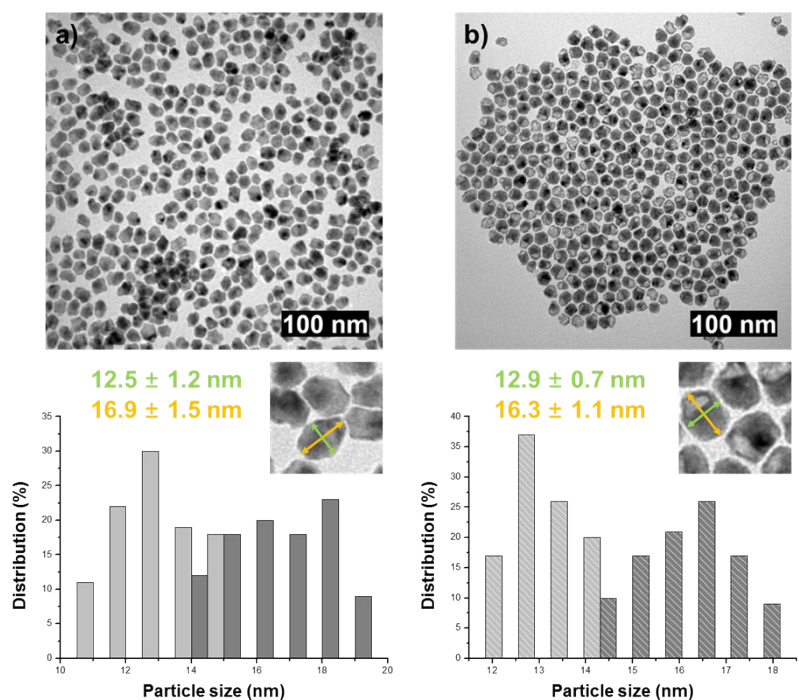


**Fig. S3** TEM images and histograms for crystal size distributions of (a) PACIN-HF and (b) ACIN-HF. The size of nanocrystal remains unchanged after the chemical etching with HCl.

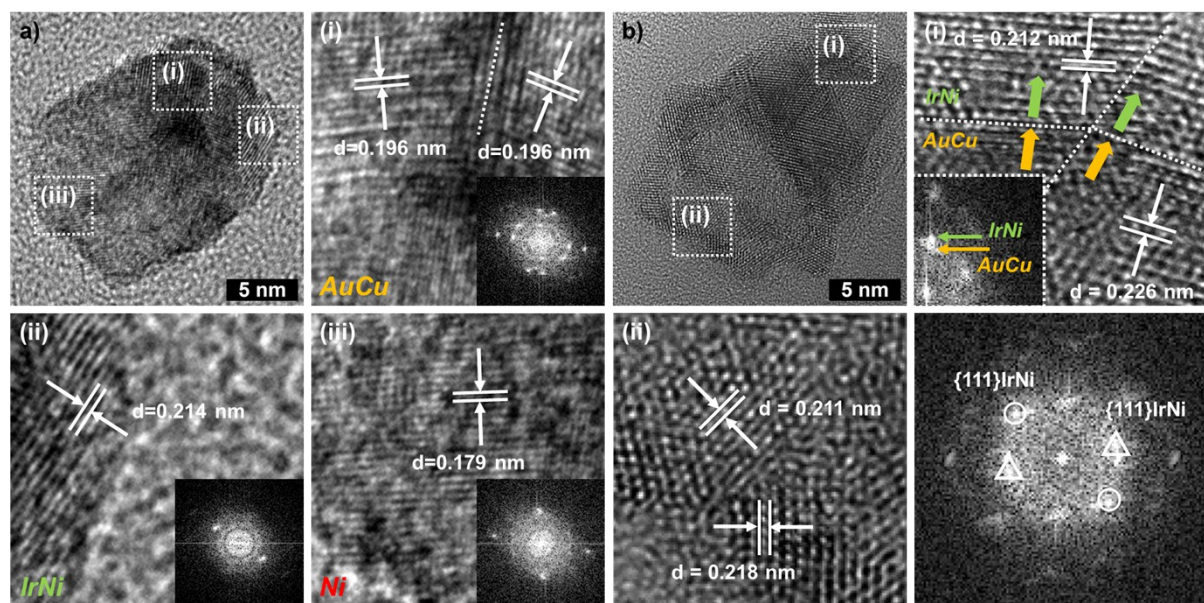


**Fig. S4** HRTEM images and corresponding FFT patterns of a) PACIN-HF and b) ACIN-HF.

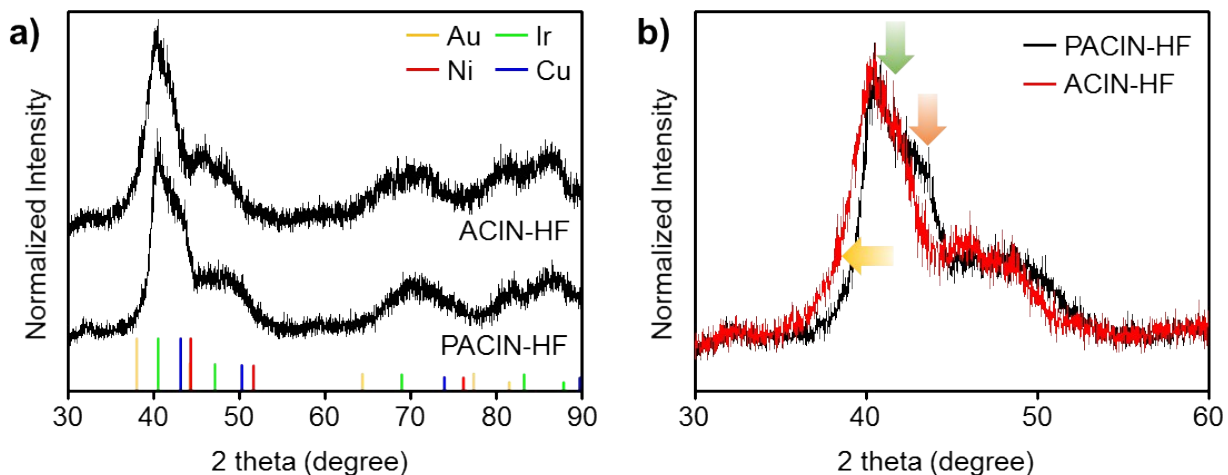


**Fig. S5** a) The XRD peaks and b) enlarged XRD peaks of PACIN-HF and ACIN-HF in order to compare the change of relative contributions of AuCu (yellow arrow), IrNi (green arrow) and Ni-rich phase (red arrow), respectively.

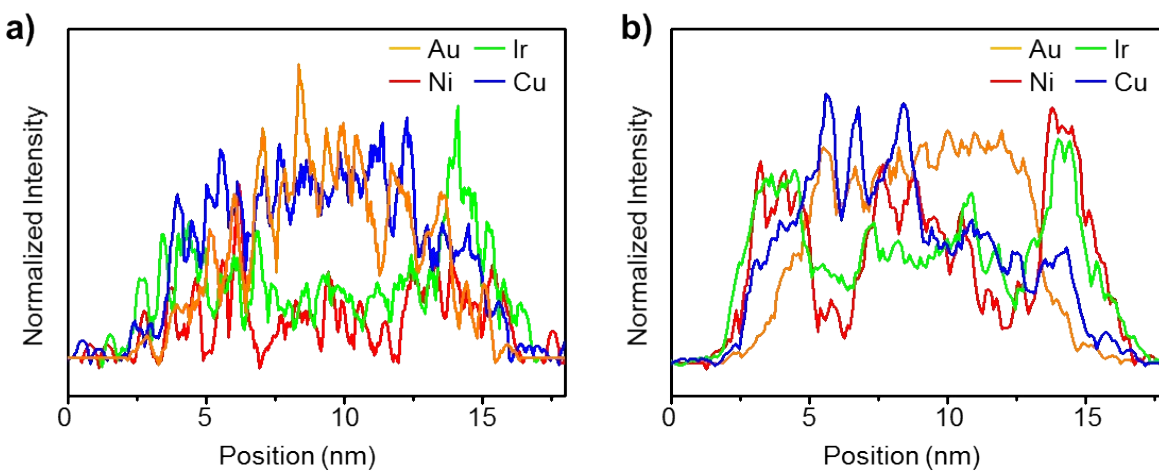


**Fig. S6** Line profile analysis of a) ACIN-CS and b) after chemical etching.

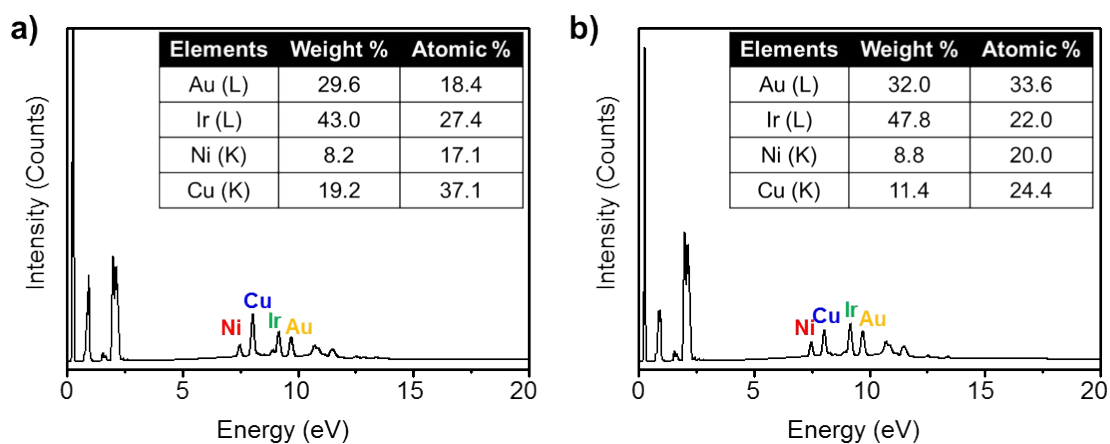


**Fig. S7** EDS spectrums of a) ACIN-CS and b) after chemical etching. Samples for EDS measurement were prepared on a Mo TEM grid.

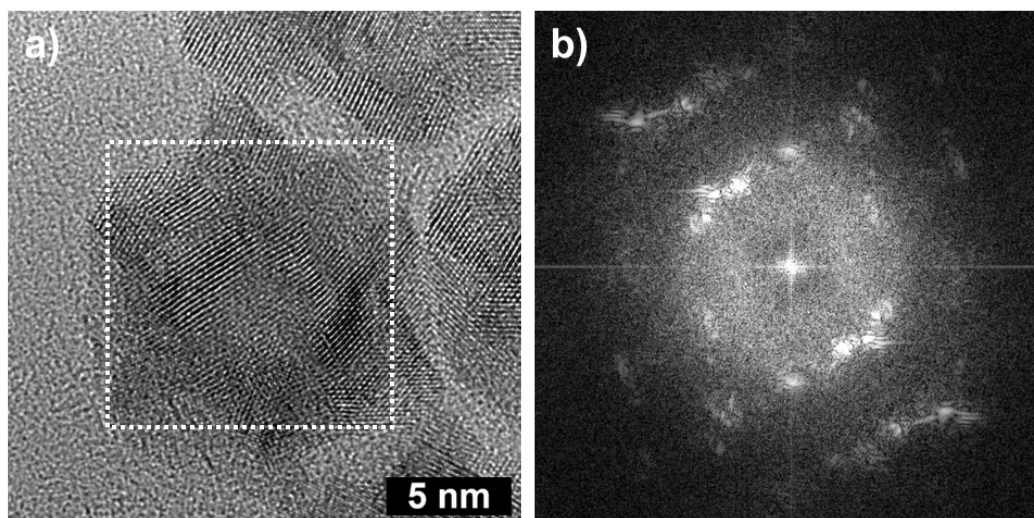


**Fig. S8** HRTEM image and corresponding FFT patterns of ACIN-CS.

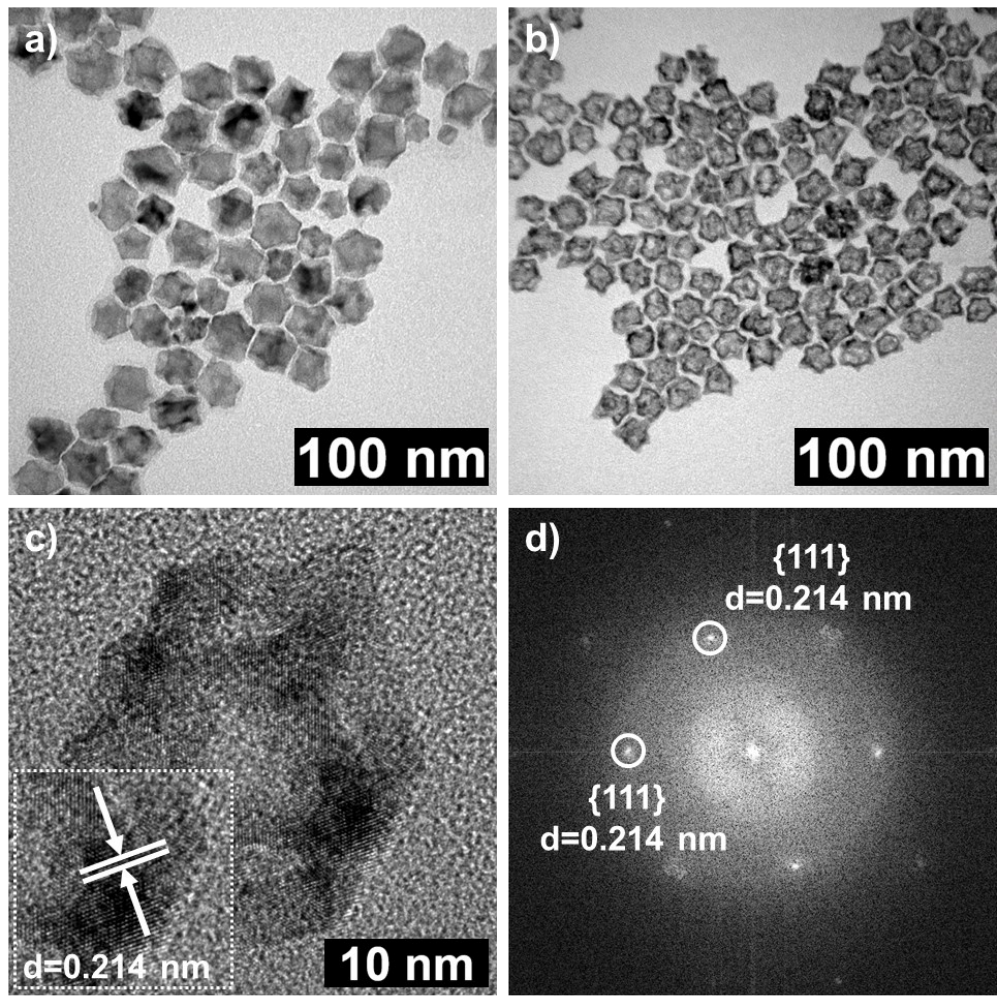


**Fig. S9** TEM images of CIN-SF a) before and b) after chemical etching process. c) HRTEM image and corresponding d) FFT pattern of CIN-SF.

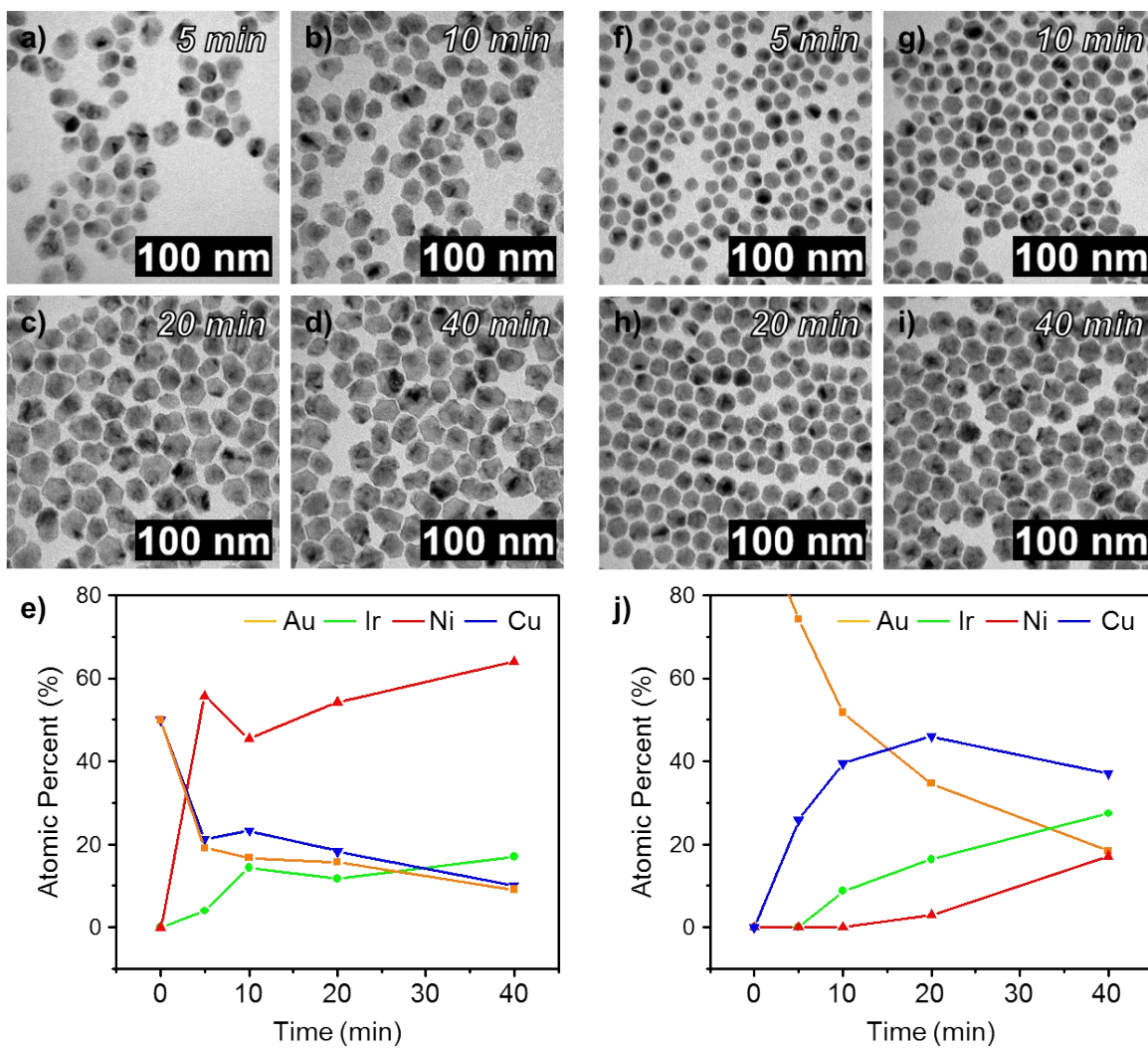


**Fig. S10** a-d) TEM images of ACIN-HF intermediates and e) corresponding EDS analyses. f-i) TEM images of ACIN-CS intermediates and j) corresponding EDS analyses.

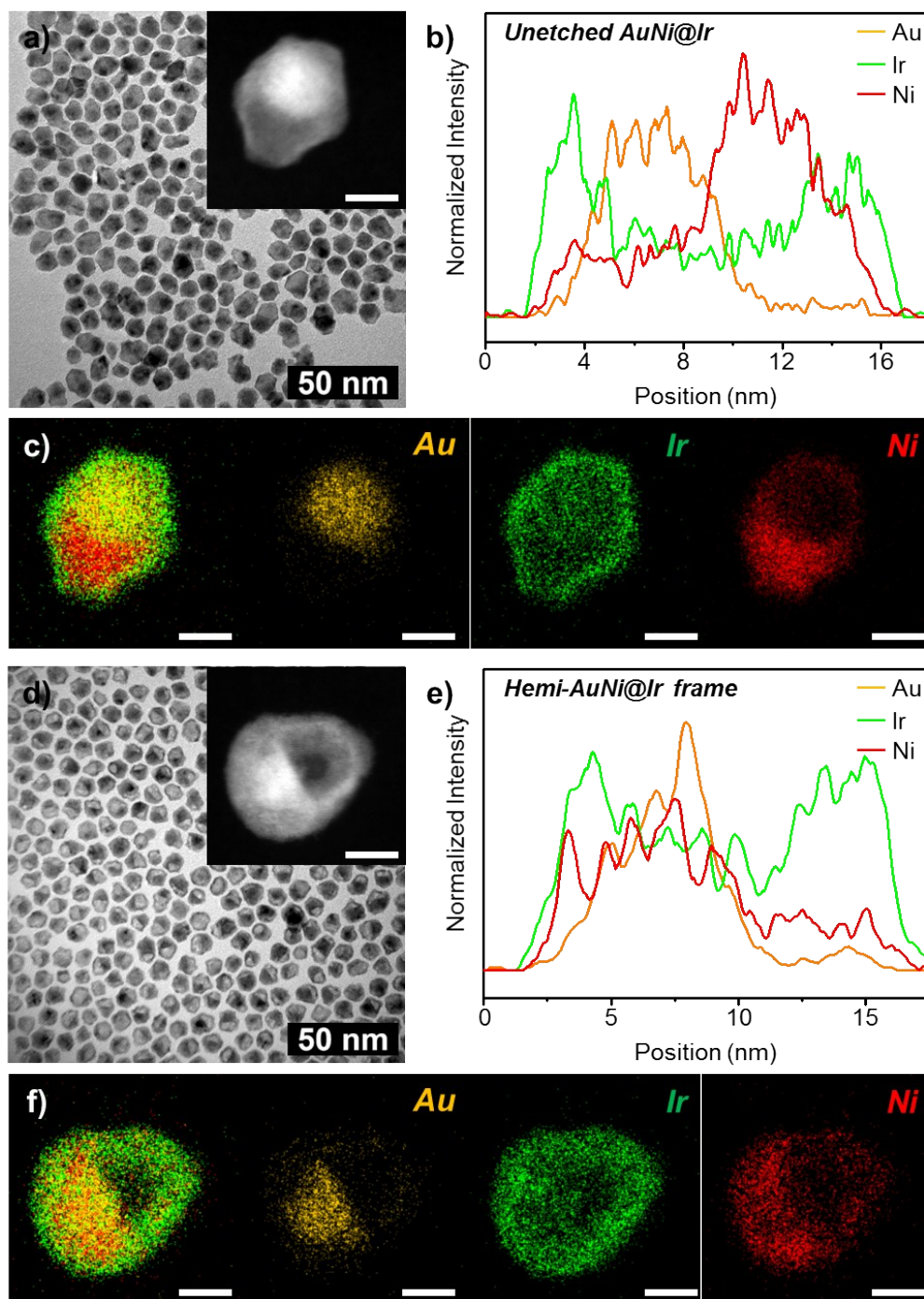


**Fig. S11** TEM images of a) unetched AuNi@Ir and d) Hemi-AuNi@Ir nanoparticles. Line profile analyses and corresponding elemental mapping analysis of b,c) unetched AuNi@Ir and e, f) Hemi-AuNi@Ir nanoparticles.

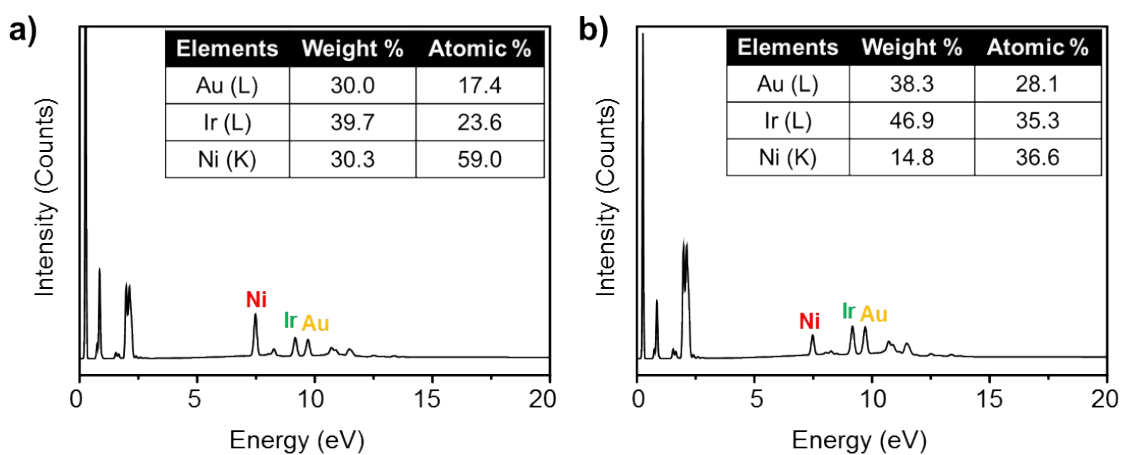


**Fig. S12** EDS spectrums of a) unetched AuNi@Ir and b) Hemi-Au@Ir frame. Samples for EDS measurement were prepared on a Mo TEM grid.

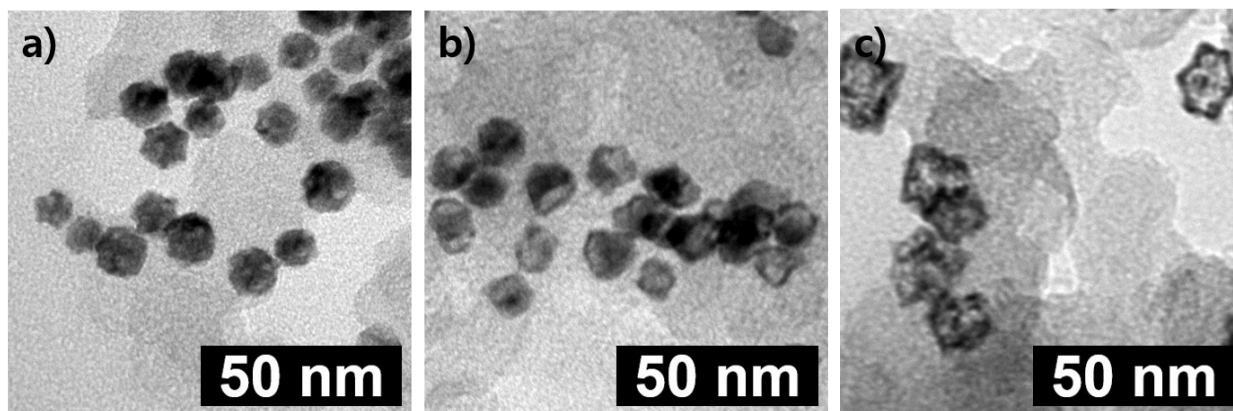


**Fig. S13** TEM images of carbon supported catalysts. (a) ACIN-CS/C, (b) ACIN-HF/C, (c) CIN-SF/C.

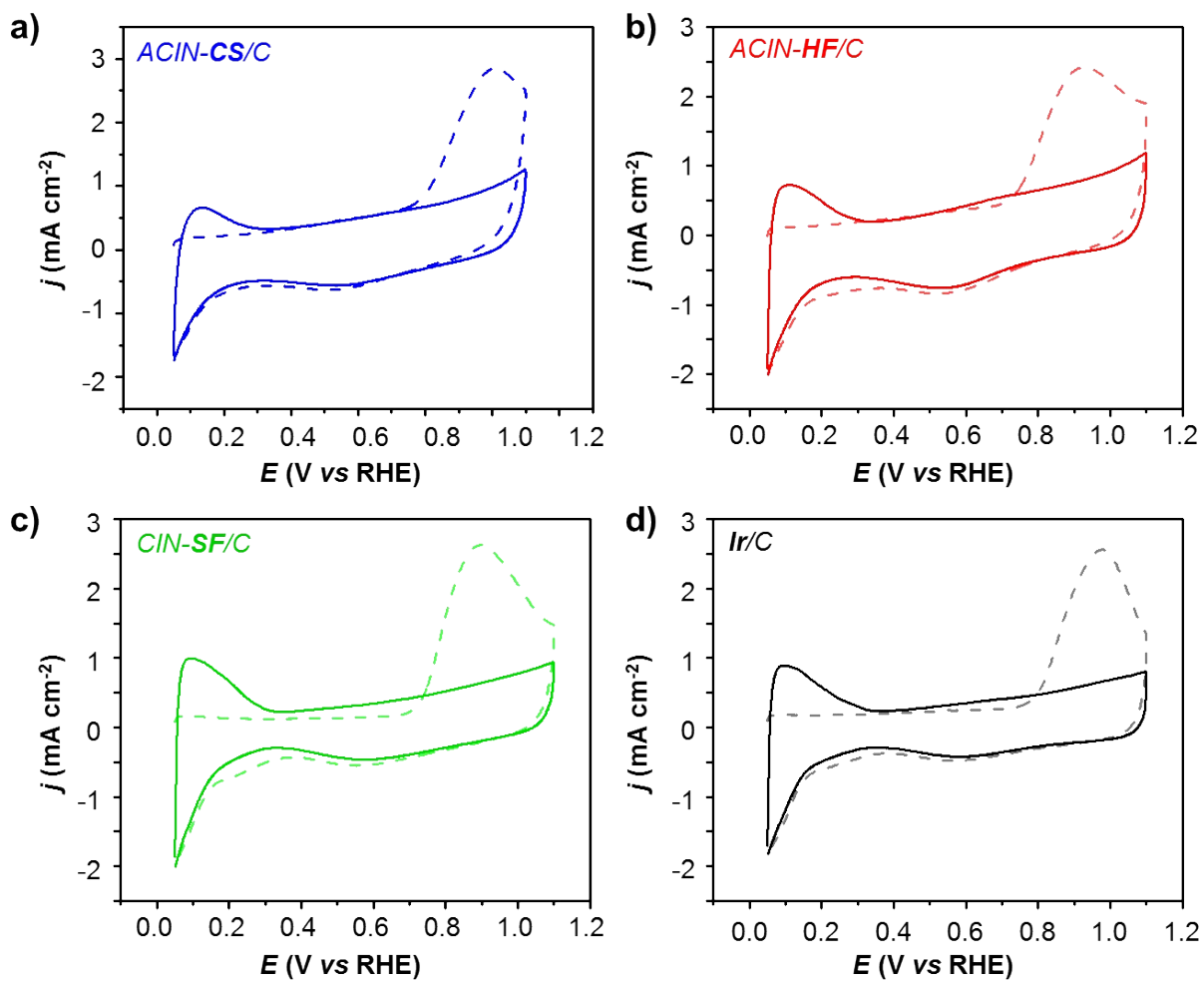


**Fig. S14** CO-stripping voltammograms (dotted line) and cyclic voltammograms (solid line) for (a) ACIN-CS/C, (b) ACIN-HF/C, (c) CIN-SF/C, and (d) Ir/C measured in 0.1 M HClO<sub>4</sub>.

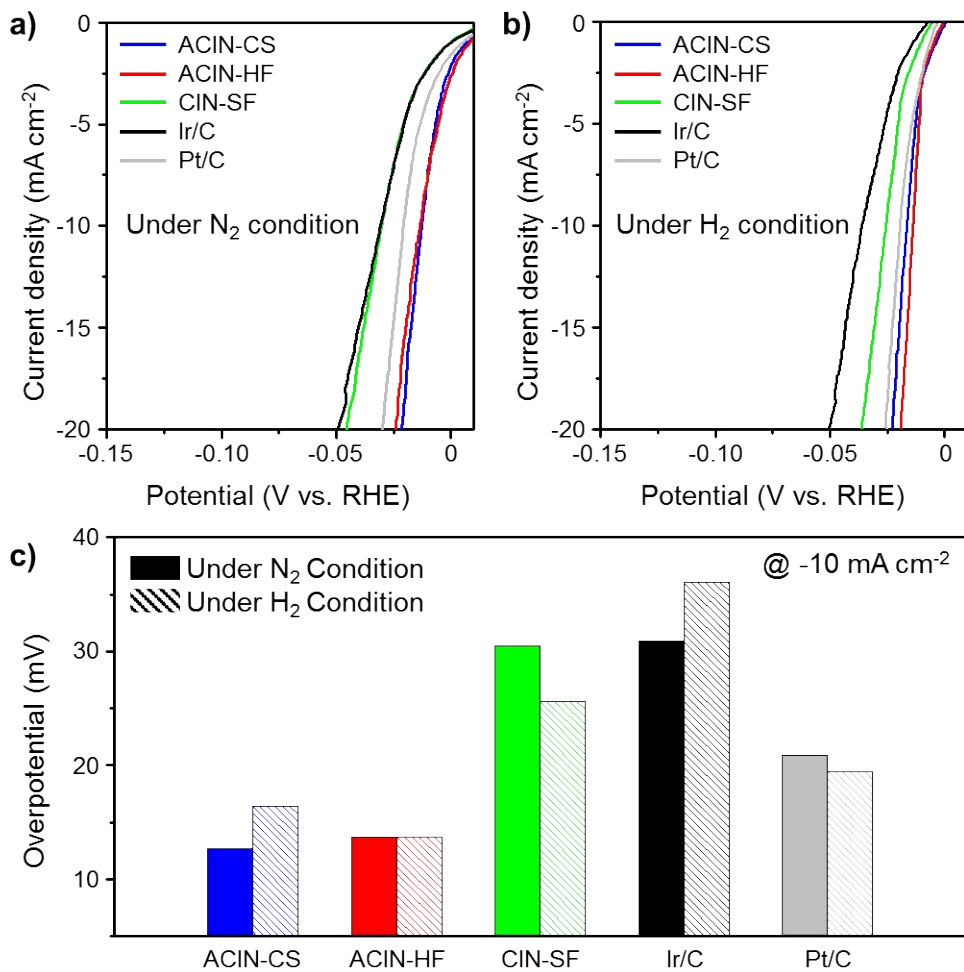


**Fig. S15** LSV curves for HER of prepared catalysts in a) N<sub>2</sub> and b) H<sub>2</sub> saturated conditions in 0.1 M HClO<sub>4</sub>. c) Comparison overpotential bar columns graph measured at -10 mA cm<sup>-2</sup>.

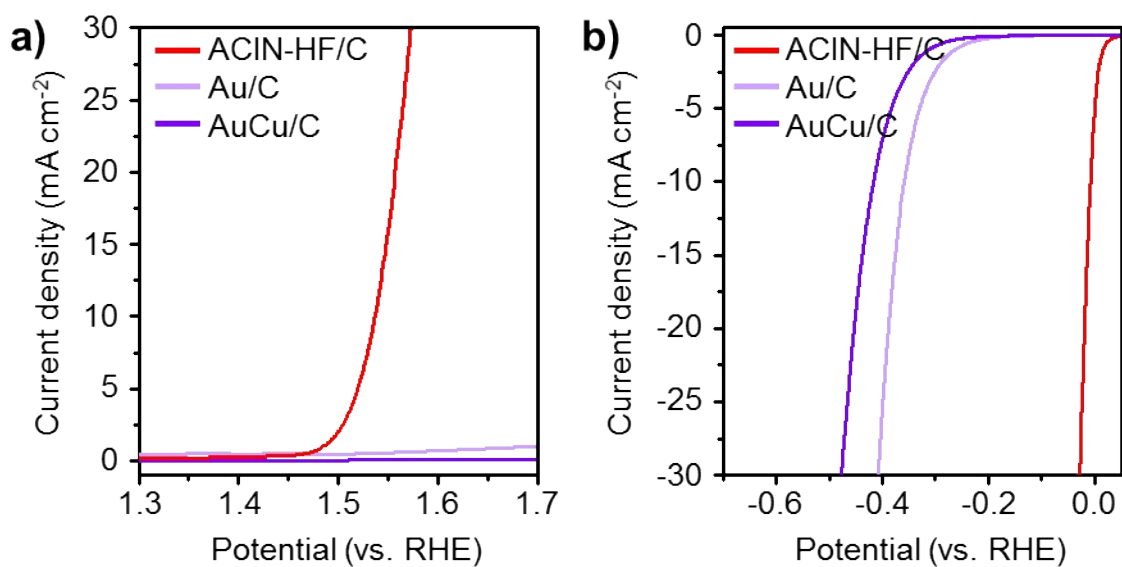


**Fig. S16** a) The OER polarization curves and b) the HER polarization curves of the ACIN-HF/C, Au/C, and AuCu/C catalysts in 0.1 M HClO<sub>4</sub> solution.

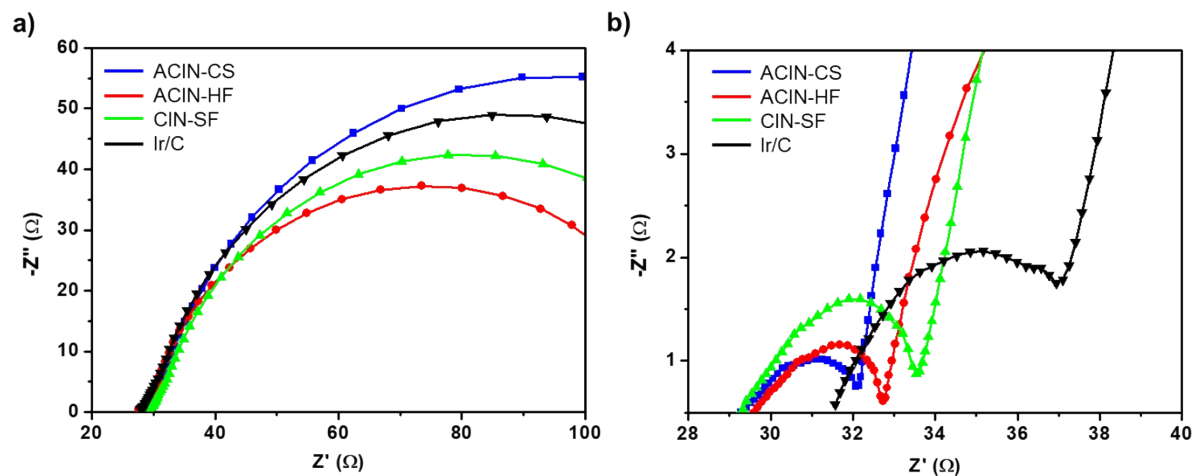


**Fig. S17** Comparison of electrochemical impedance spectroscopy (EIS) Nyquist plots in 0.1 M HClO<sub>4</sub>. Impedance spectra of a) OER and b) HER.

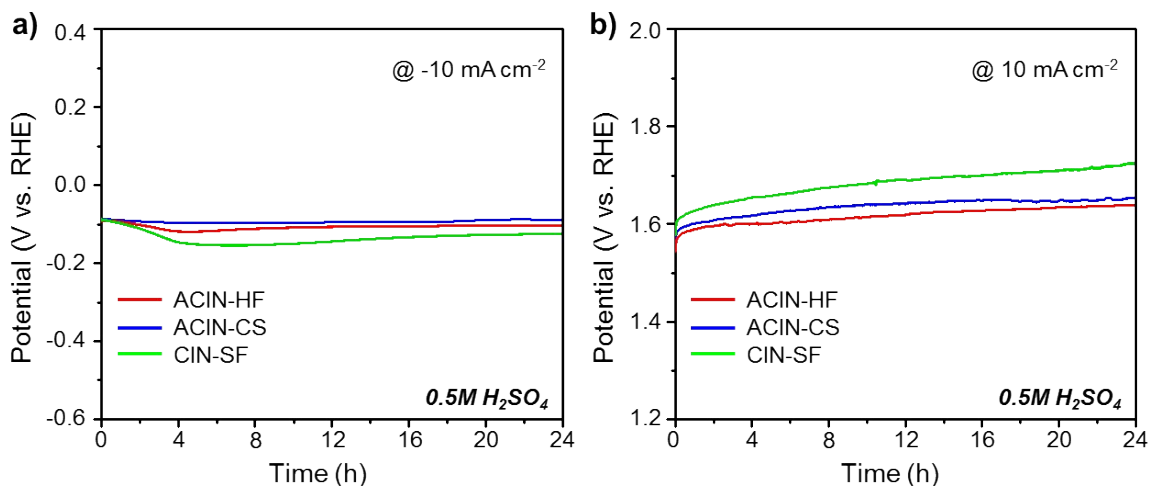


**Fig. S18** Chronopotentiometry tests of synthesized nanocrystals at  $-10 \text{ mA cm}^{-2}$  in  $0.5 \text{ M H}_2\text{SO}_4$  solution for a) HER and at  $10 \text{ mA cm}^{-2}$  in  $0.5 \text{ M H}_2\text{SO}_4$  for b) OER.

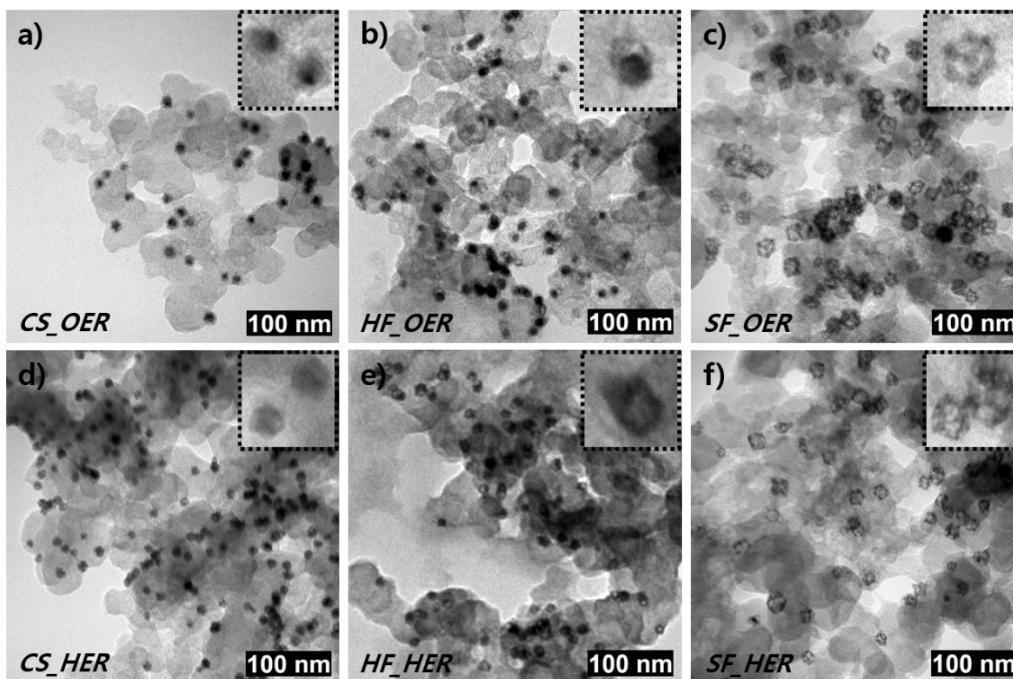


**Fig. S19** a, b, c) TEM images of ACIN-CS/C, ACIN-HF/C, and CIN-SF after chronopotentiometry test for OER at  $10 \text{ mA cm}^{-2}$  in  $0.5 \text{ M H}_2\text{SO}_4$  solution respectively. d, e, f) TEM images of ACIN-CS/C, ACIN-HF/C, and CIN-SF/C after chronopotentiometry test for HER at  $-10 \text{ mA cm}^{-2}$  in  $0.5 \text{ M H}_2\text{SO}_4$  solution, respectively. Inset images are enlarged TEM images of each catalysts.

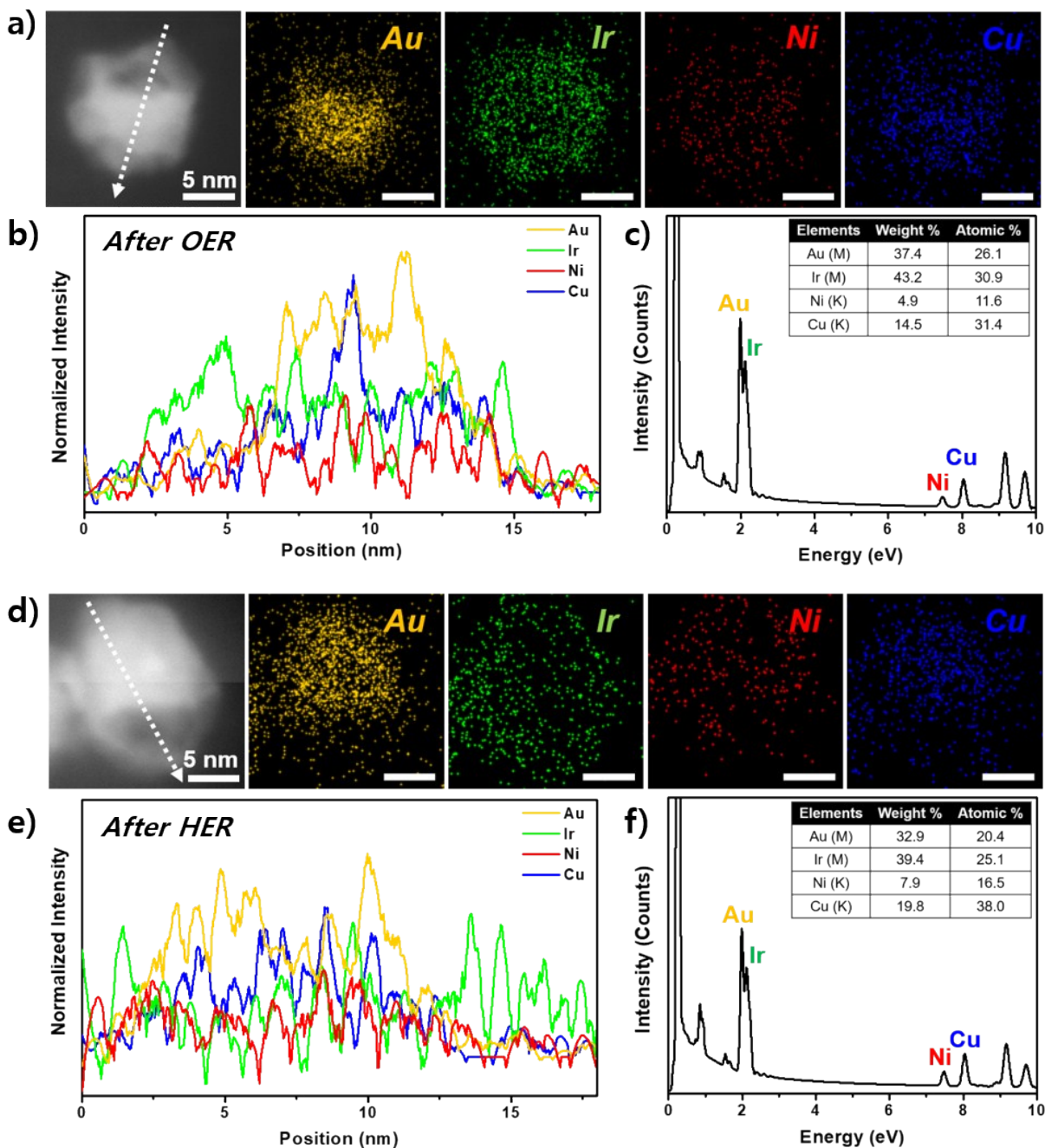


**Fig. S20** a, d) STEM images and their corresponding elemental mapping data of ACIN-HF/C after chronopotentiometry test for OER and HER at  $10 \text{ mA cm}^{-2}$  and  $-10 \text{ mA cm}^{-2}$  in  $0.5 \text{ M H}_2\text{SO}_4$  solution, respectively. b, e) line profiles and c, f) EDS spectrum of ACIN-HF/C after chronopotentiometry test for OER and HER, respectively.

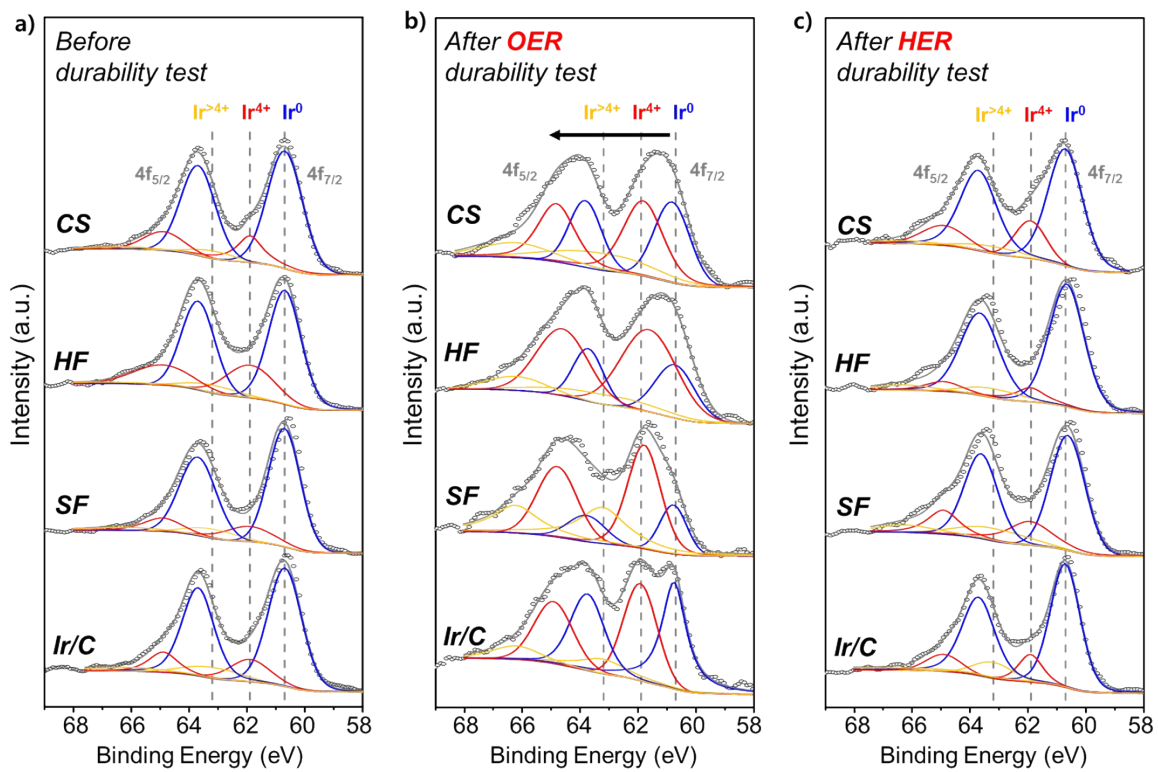


**Fig. S21** Ir 4f XPS spectra for ACIN-CS/CFP, ACIN-HF/CFP, CIN-SF/CFP, and Ir/C/CFP catalysts (a) before durability test, (b) after OER durability test, and (c) after HER durability test.

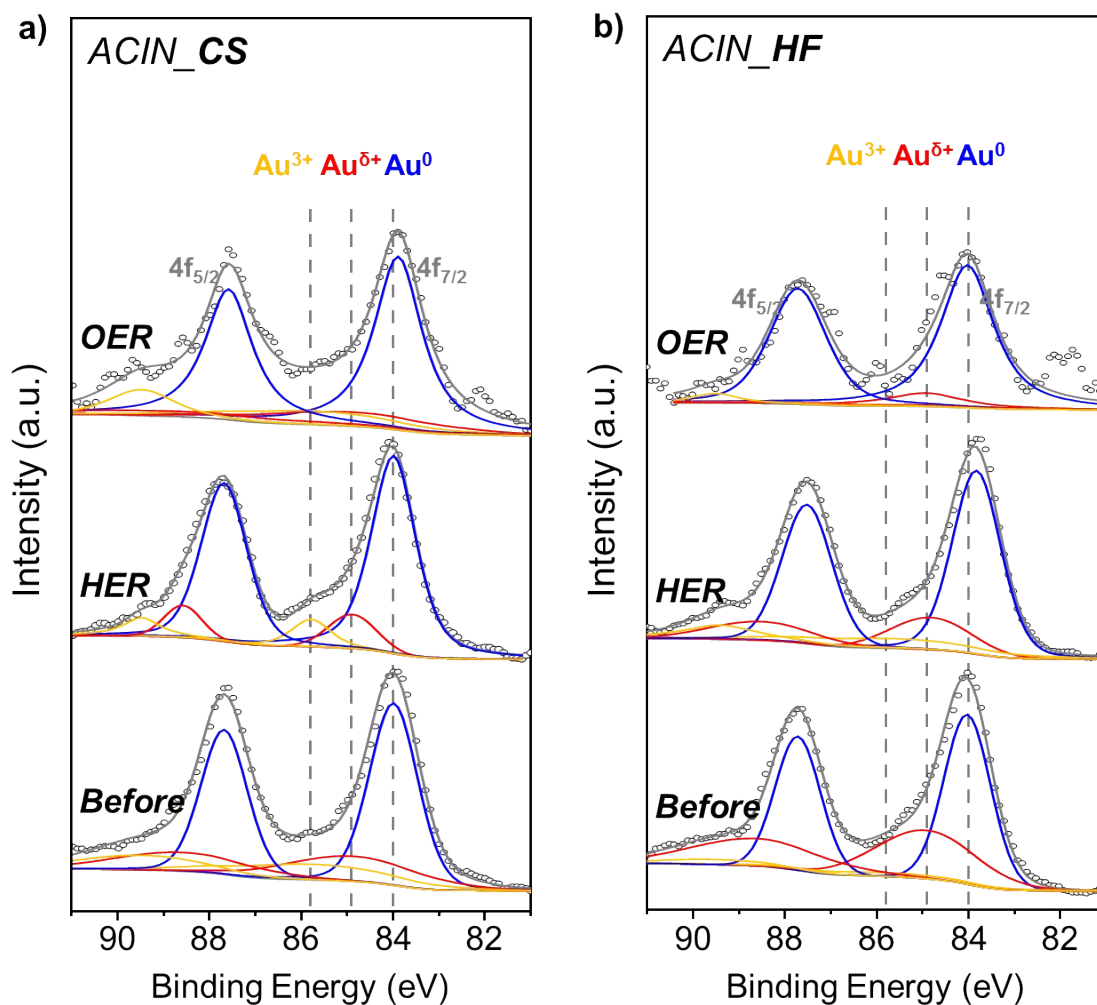


**Fig. S22** Au 4f XPS spectra for (a) ACIN-CS/CFP, and (b) ACIN-HF/CFP. Each spectra of catalyst show the XPS of the gold before durability test, after HER durability test, and OER test.

**Table S1.** Metal contents in ACIN-HF/C, ACIN-CS/C, and CIN-SF/C catalysts determined by ICP-AES analysis.

Sample	Weight Percent (%)				Atomic Percent (%)			
	Au	Ir	Ni	Cu	Au	Ir	Ni	Cu
ACIN-HF/C	34.1	51.9	9.5	4.5	25.5	40.0	24.0	10.5
ACIN-CS/C	32.7	51.6	8.3	7.4	23.9	38.8	20.5	16.8
CIN-SF/C	-	87.7	11.4	0.8	-	68.7	29.3	2.0

**Table S2.** Full cell activity comparison table showing the catalyst loading and overpotential.

Catalyst	Mass Loading ( $\mu\text{g}_{\text{Ir}} \text{cm}^{-2}$ )	Electrolyte	Current Density ( $\text{mA cm}^{-2}$ )	Overpotential ( $\eta$ ) (mV vs. RHE)	Ref.
ACIN-HF	~100	0.5 M H <sub>2</sub> SO <sub>4</sub>	10	355	This work
ACIN-CS	~100	0.5 M H <sub>2</sub> SO <sub>4</sub>	10	367	This work
CIN-SF	~100	0.5 M H <sub>2</sub> SO <sub>4</sub>	10	373	This work
Ir/CFP	~100	0.5 M H <sub>2</sub> SO <sub>4</sub>	10	381	
IrCoNi-PHNC	-	0.5 M H <sub>2</sub> SO <sub>4</sub>	10	~420	1
IrNi NCs	-	0.5 M H <sub>2</sub> SO <sub>4</sub>	10	~345	2
IrNiFe NPs	200	0.5 M HClO <sub>4</sub>	10	390	3
Ir WNWs	30.6	0.5 M HClO <sub>4</sub>	10	~380	4
			20	~440	

- Not available to identify

~ Estimated values

**Table S3.** OER activity comparison table showing the catalyst loading and overpotential.

Catalyst	Mass Loading ( $\mu\text{g}_{\text{Ir}} \text{cm}^{-2}$ )	Electrolyte	Current Density ( $\text{mA cm}^{-2}$ )	Overpotential ( $\eta$ ) (mV vs. RHE)	Ref.
AuCuIrNi-HF	~10	0.1 M HClO <sub>4</sub>	10	308	This work
AuCuIrNi-CS	~10	0.1 M HClO <sub>4</sub>	10	318	This work
IrCoNi PHNC	10	0.1 M HClO <sub>4</sub>	10	303	1
IrNi NCs	12.5	0.1 M HClO <sub>4</sub> 0.1 M KOH	10	280 270	2
IrNiFe NPs	92	0.5 M HClO <sub>4</sub>	10	284	3
Ir WNWs	~31	0.5 M HClO <sub>4</sub> 0.1 M HClO <sub>4</sub>	10	270 280	4
Co-IrCu ONC/C	20	0.1 M HClO <sub>4</sub>	10	290	5
IrNiCu DNF/C	20	0.1 M HClO <sub>4</sub>	10	300	6
IrO <sub>x</sub> -Ir	133	0.5 M HClO <sub>4</sub>	10	295	7
Ir/Au	-	0.1 M H <sub>2</sub> SO <sub>4</sub>	10	410	8
IrNi-RF/C	-	0.1 M HClO <sub>4</sub>	10	313.6	9
IrNiO <sub>x</sub> /ATO	10.2	0.05 M H <sub>2</sub> SO <sub>4</sub>	10	360	10
IrNi oxide	~20	0.1 M HClO <sub>4</sub>	10	310	11
Ir	-	1 M H <sub>2</sub> SO <sub>4</sub> 1 M KOH	10	360 430	12
Ru	-	1 M H <sub>2</sub> SO <sub>4</sub> 1 M KOH	10	340 320	12
IrO <sub>x</sub> /SrIrO <sub>3</sub>	-	0.5 M H <sub>2</sub> SO <sub>4</sub>	10	275	13
Ir <sub>0.7</sub> Ru <sub>0.3</sub> O <sub>x</sub>	60 $\mu\text{g cm}^{-2}$	0.05 M H <sub>2</sub> SO <sub>4</sub>	100 A g <sup>-1</sup> <sub>oxides</sub>	270	14

- Not available to identify

~ Estimated values

**Table S4.** HER activity comparison table showing the catalyst loading and overpotential.

Catalyst	Mass Loading ( $\mu\text{g}_{\text{Ir}} \text{cm}^{-2}$ )	Electrolyte	Current Density ( $\text{mA cm}^{-2}$ )	Overpotential ( $\eta$ ) (mV vs. RHE)	Ref.
<b>AuCuIrNi-HF</b>	~10	0.1 M HClO <sub>4</sub>	-10	23.7	<b>This work</b>
<b>AuCuIrNi-CS</b>	~10	0.1 M HClO <sub>4</sub>	-10	22.7	<b>This work</b>
<b>IrCoNi-PHNC</b>	10	0.1 M HClO <sub>4</sub>	-10 -20	33 56	1
<b>IrCo-PHNC</b>	10	0.1 M HClO <sub>4</sub>	-10 -20	21 35	1
<b>IrNi NCs</b>	12.5	0.1 M HClO <sub>4</sub> 0.5 M H <sub>2</sub> SO <sub>4</sub>	-20	21 32	2
<b>IrNiFe NPs</b>	92	0.5 M HClO <sub>4</sub>	-10	24	3
<b>Ir WNWs</b>	~31	0.5 M HClO <sub>4</sub>	-10 -20	15 19	4
	~31	0.1 M HClO <sub>4</sub>	-10 -20	11 14	4
<b>Ru@C<sub>2</sub>N</b>	0.285 mg cm <sup>-2</sup>	0.5 M H <sub>2</sub> SO <sub>4</sub>	-10 -20	22 34.8	15
<b>Rh<sub>2</sub>P</b>	13.3 $\mu\text{g}_{\text{Rh}} \text{cm}^{-2}$	0.5 M H <sub>2</sub> SO <sub>4</sub>	-10	~20	16
<b>Au@PdAg NRBs</b>	12.7 $\mu\text{g}_{\text{Pd}} \text{cm}^{-2}$	0.5 M H <sub>2</sub> SO <sub>4</sub>	-10	26.2	17
<b>RuP<sub>2</sub>@NPC</b>	1.0 mg cm <sup>-2</sup>	0.5 M H <sub>2</sub> SO <sub>4</sub>	-10	38	18
<b>IrNiN NPs</b>	-	0.1 M HClO <sub>4</sub>	-6	110	19
<b>IrO<sub>2</sub>-Fe<sub>2</sub>O<sub>3</sub></b>	0.125 mg cm <sup>-2</sup>	0.5 M H <sub>2</sub> SO <sub>4</sub>	-10	78	20
<b>IrO<sub>2</sub>-TiO<sub>2</sub></b>	-	0.5 M H <sub>2</sub> SO <sub>4</sub>	-10	112	21
<b>Ru/C<sub>3</sub>N<sub>4</sub>/C</b>	204 $\mu\text{g cm}^{-2}$	0.5 M H <sub>2</sub> SO <sub>4</sub>	-10	70	22
<b>Pt<sub>3</sub>Ni<sub>3</sub> NWs</b>	15.3 $\mu\text{g}_{\text{Pt}} \text{cm}^{-2}$	0.5 M H <sub>2</sub> SO <sub>4</sub>	-10	~30	23

- Not available to identify

~ Estimated values

**Table S5.** Metal contents in electrolytes after the durability test.

<b>Samples</b>	<b>After HER</b>		<b>After OER</b>	
	Ni (ppm)	Cu (ppm)	Ni (ppm)	Cu (ppm)
ACIN-CS/C	0.136	0.043	0.282	0.114
ACIN-HF/C	0.192	0.006	0.251	0.071
CIN-SF/C	0.074	< 0.005	0.218	0.006

## References

- S1. J. Feng, F. Lv, W. Zhang, P. Li, K. Wang, C. Yang, B. Wang, Y. Yang, J. Zhou, F. Lin, G.-C. Wang and S. Guo, *Adv. Mater.*, 2017, **29**, 1703798
- S2. Y. Pi, Q. Shao, P. Wang, J. Guo and X. Huang, *Adv. Funct. Mater.*, 2017, **27**, 1700886
- S3. L. Fu, G. Cheng and W. Luo, *J. Mater. Chem. A.*, 2017, **5**, 24836-24841
- S4. L. Fu, F. Yang, G. Cheng and W. Luo, *Nanosclae*, 2018, **10**, 1892-1897
- S5. T. Kwon, H. Hwang, Y. J. Sa, J. Park, H. Baik, S. H. Joo and K. Lee, *Adv. Funct. Mater.*, 2017, **27**, 1604688
- S6. J. Park, Y. J. Sa, H. Baik, T. Kwon, S. H. Joo and K. Lee, *ACS Nano*, 2017, **11**, 5500-5509
- S7. P. Lettenmeier, L. Wang, U. Golla-Schindler, P. Gazdzicki, N. A. Cañas, M. Handl, R. Hiesgen, S. S. Hosseiny, A. S. Gago and K. A. Friedrich, *Angew. Chem. Int. Ed.*, 2016, **55**, 742-746
- S8. S. H. Ahn, H. Tan, M. Haensch, Y. Liu, L. A. Bendersky and T. P. Moffat, *Energy Environ. Sci.*, 2015, **8**, 3557-3562
- S9. H. Jin, Y. Hong, J. Yoon, A. Oh, N. K. Chaudhari, H. Baik, S. H. Joo and K. Lee, *Nano Energy*, 2017, **42**, 17-25
- S10. H. N. Nong, H.-S Oh, T. Reier, E. Willinger, M.-G. Willinger, V. Petkov, D. Teschner and P. Strasser, *Angew. Chem. Int. Ed.*, 2015, **54**, 2975
- S11. T. Reier, Z. Pawolek, S. Cherevko, M. Bruns, T. Jones, D. Teschner, S. Selve, A. Bergmann, H. N. Nong, R. Schlögl, K. J. J. Mayrhofer and P. Strasser, *J. Am. Chem. Soc.*, 2015, **137**, 13031-13040
- S12. C. C. L. McCrory, S. Jung, I. M. Ferrer, S. M. Chatman, J. C. Peters and T. F. Jaramillo, *J. Am. Chem. Soc.* 2015, **137**, 4347-4357
- S13. L. C. Seitz, C. F. Dickens, K. Nishio, Y. Hikita, J. Montoya, A. Doyle, C. Kirk, A. Vojvodic, H. Y. Hwang, J. K. Norskov and T. F. Jaramillo, *Science*, 2016, **353**, 1011-1014

- S14. L. Wang, V. A. Saveleva, S. Zafeiratos, E. R. Savinova, P. Lettenmeler, P. Gazdzicki, A. S. Gago and K. A. Friedrich, *Nano Energy*, 2017, **34**, 385-391
- S15. J. Mahmood, F. Li, S.-M. Jung, M. S. Okyay, I. Ahmad, S. J. Kim, N. Park, H. Y. Jeong and J.-B Baek, *Nat. Nanotechnol.* 2017, **12**, 441-446
- S16. H. Duan, D. Li, Y. Tang, Y. He, S. Ji, R. Wang, H. Lv, P. P. Lopes, A. P. Paulikas, H. Li, S. X. Mao, C. Wang, N. M. Markovic, J. Li, V. R. Stamenkovic and Y. Li, *J. Am. Chem. Soc.*, 2017, **139**, 5494
- S17. Z. Fan, Z. Luo, X. Huang, B. Li, Y. Chen, J. Wang, Y. Hu and H. Zhang, *J. Am. Chem. Soc.*, 2016, **138**, 1414-1419
- S18. Z. Pu, I. S. Amiin, Z. Kou, W. Li and S. Mu, *Angew. Chem. Int. Ed.*, 2017, **56**, 11559-11564
- S19. K. A. Kuttiyiel, K. Sasaki W.-F. Chen, D. Su and R. R. Adzic, *J. Mater. Chem. A*, 2014, **2**, 591-594
- S20. X. Yang, Y. Li, L. Deng, W. Li, Z. Ren, M. Yang, X. Yang and Y. Zhu, *RSC Adv.*, 2017, **7**, 20252-20258
- S21. M. Yuan, Y. Zhu, L. Deng, R. Ming, A. Zhang, W. Li, B. Chai and Z. Ren, *New J. Chem.*, 2017, **41**, 6152-6159
- S22. Y. Zheng, Y. Jiao, Y. Zhu, L. H. Li, Y. Han, Y. Chen, M. Jaroniec and S.-Z. Qiao, *J. Am. Chem. Soc.*, 2016, **138**, 16174-16181
- S23. P. Wang, K. Jiang, G. Wang, J. Yao and X. Huang, *Angew. Chem.* 2016, **128**, 13051-13055